Electronic supplementary information

A green approach to the fabrication of TiO_2/NiAl-LDH core–shell hybrid photocatalyst for efficient and selective solar-powered reduction of CO_2 into value-added fuels

Wan-Kuen Jo, [a] Satyanarayana Moru, [b] Surendar Tonda [a,*]

[a] Department of Environmental Engineering, Kyungpook National University, 80 Daehak-ro, Buk-gu, Daegu 41566, Republic of Korea.

[b] Department of Electrical and Computer Engineering, Iowa State University, Coover Hall, Osborn Drive, Ames, Iowa 50011, USA.

Corresponding Author:

S. Tonda, E-mail: surendar.t86@gmail.com; surendart@knu.ac.kr

Contact No.: +82 53 950 6584.

Experimental section

Materials

Agarose, titanium(IV) oxysulfate, nickel(II) nitrate hexahydrate, aluminum nitrate nonahydrate, ammonium fluoride, and urea were purchased from Sigma-Aldrich. All other chemicals used in this study were of analytical reagent grade and were used without further purification. The deionized water used in this study was obtained from a Wellix Plus water purification system.

Material characterization

The surface morphology of the synthesized samples was examined by field-emission scanning electron microscopy (FESEM, Hitachi SU8220). The detailed microstructure of the samples was explored by transmission electron microscopy (TEM, Hitachi HT 7700) and field-emission TEM (FETEM, Titan G2 ChemiSTEM Cs Probe (FEI Company, The Netherlands)) in conjunction with energy-dispersive X-ray spectroscopy (EDS). Powder X-ray diffraction (XRD) analysis was performed with a Rigaku (D/Max-2500) diffractometer equipped with a Cu-K_α radiation source (λ = 1.5406 Å). The samples were analyzed by ultraviolet–visible diffuse-reflectance spectroscopy (UV–Vis DRS) conducted on a Shimadzu UV-2600 UV–Vis spectrophotometer using $BaSO_4$ as a reference sample. Fourier-transform infrared (FT-IR) spectra were collected on a PerkinElmer (Frontier) FT-IR/NIR spectrometer. The thermal behaviors of the catalysts were determined by thermogravimetric analysis (TGA) on a TA Instruments Q500 analyzer. Photoluminescence (PL) spectra were recorded at an excitation wavelength of 380 nm using a Shimadzu RF-6000 spectrofluorophotometer. The surface electronic states of the samples were examined by X-ray photoelectron spectroscopy (XPS) using a Thermo Scientific K-Alpha X-ray photoelectron spectrometer. Nitrogen adsorption–desorption isotherm measurements were performed on a BELSORP-max (Japan) apparatus at liquid-N_2 temperature. CO_2 adsorption isotherms were recorded on a BELSORP-max (Japan) at 298 K. The electron spin resonance (ESR) measurements were recorded on a Bruker EMXplus-9.5/2.7 spectrometer.

Transient photocurrent and electrochemical impedance spectroscopy measurements

Transient photocurrent and EIS measurements were performed on an IVIUM Technologies electrochemical workstation using a three-electrode cell. Indium tin oxide (ITO) coated with a catalyst served as the working electrode; Ag/AgCl (in saturated KCl) and Pt foil served as the

reference and counter electrodes, respectively. A 300 W Xe lamp was used as the light source in experiments to measure the transient photocurrent responses of the synthesized catalysts, and an aqueous Na_2SO_4 (0.5 M) solution was used as the supporting electrolyte. Electrochemical impedance spectroscopy (EIS) measurements were performed at an open-circuit potential with a sinusoidal ac perturbation of 10 mV over the frequency range from 10 mHz to 100 kHz; these experiments were conducted with 10 mM $K_3[Fe(CN)_6]$ containing KCl (0.1 M) solution. For the preparation of the working electrode, 15 mg of the as-synthesized catalyst was suspended in 20 μL of Nafion solution (5 wt%) and 0.5 mL of ethanol. The obtained mixture was ground to form a slurry, which was then evenly spread as a thin film onto an ITO glass substrate with an active area of 1.0 cm^2. The coated ITO substrate was then dried in an oven at 80 °C.

Photocatalytic CO_2 reduction tests

Photocatalytic CO_2 reduction experiments were conducted in a homemade stainless steel reactor (80 mL) with a quartz window at the top for the transmission of light. A 300 W Xe arc lamp (spectral output shown in Fig. S1) with a focused intensity of ca. 150 mW cm^{-2} was used as the light source to trigger the CO_2 reduction reaction. In a typical process, 50 mg of the catalyst powder was evenly distributed on a circular glass dish and placed at the bottom of the stainless-steel reactor. Three hundred microliters of degassed and CO_2-saturated water (to remove any dissolved O_2) was introduced into the reactor for humidity and electron donation. Prior to illumination, the reactor was vacuum-treated and purged with high-purity CO_2 gas for 1 h to ensure that air was completely removed from the reactor. After this process was completed, the reactor was backfilled with CO_2 gas to maintain an inside pressure of approximately 1 bar. The temperature of the system was held constant at 80 °C to generate water vapor. The pressure and temperature inside the system were continuously monitored using a dial pressure gauge. During the irradiation, 500 μL of gas was periodically extracted from the reactor for quantitative analysis of the products on a Shimadzu Tracera GC-2010 Plus gas chromatograph equipped with barrier ionization detector and He as a carrier gas. The quantification of the production yield was based on a calibration curve of a standard gas mixture. Isotope-labeled experiments were performed with $^{13}CO_2$ instead of $^{12}CO_2$, and the resultant products were analyzed via gas chromatography–mass spectrometry (GC–MS, Clarus 680 and Clarus SQ8T, PerkinElmer; Carboxen-1010 column).

The selectivity toward the formation of CO, CH_4, and H_2 were simply deduced according to the following equations:

$$CH_4\ selectivity\ (\%) = \frac{8N_{CH_4}}{8N_{CH_4} + 2N_{CO} + 2N_{H_2}} \times 100$$

$$CO\ selectivity\ (\%) = \frac{2N_{CO}}{8N_{CH_4} + 2N_{CO} + 2N_{H_2}} \times 100$$

$$H_2\ selectivity\ (\%) = \frac{2N_{H_2}}{8N_{CH_4} + 2N_{CO} + 2N_{H_2}} \times 100$$

where N_{CH_4}, N_{CO}, and N_{H_2} are the yields of CH_4, CO, and H_2, respectively.

The apparent quantum yield (AQY) of the photocatalyst was calculated using the following equations:

$$AQY\ (\%) = \frac{number\ of\ reacted\ electrons}{number\ of\ incident\ photons} \times 100\ \%$$

$$AQY\ of\ CH_4\ (\%) = \frac{8\ x\ number\ of\ CH_4\ molecules}{number\ of\ incident\ photons} \times 100\ \%$$

$$Moles\ of\ incident\ photons\ (N_{Einstein}) = \frac{number\ of\ incident\ photons\ (N_p)}{N_A}$$

$(N_A = Avogadro\ number = 6.02\ \times\ 10^{23})$

Number of incident photons N_p can be calculated by

$$N_P = \frac{E}{E_P}\ and,\ Photon\ energy\ (E_P) = \frac{hc}{\lambda}$$

Irradiance (E) = light intensity $(mW.cm^{-2})$ × effective light irradiation area (cm^2)

$$N_P = \frac{E\lambda}{hc} \times \frac{1}{N_A}$$

$$h = 6.626\ \times\ 10^{-34} J.sec$$

$$c = 3\ \times\ 10^8\ m.sec^{-1}$$

$$\lambda = wavelength\ (nm)$$

$$For\ example, irradiation\ time = 5\ h = 5\ \times\ 3600\ sec$$

$$AQY\ of\ CH_4\ (\%) = \frac{8\ \times CH_4\ (moles)\ \times\ N_A\ \times\ hc}{E\lambda\ \times\ irradiation\ time} \times 100\ \%$$

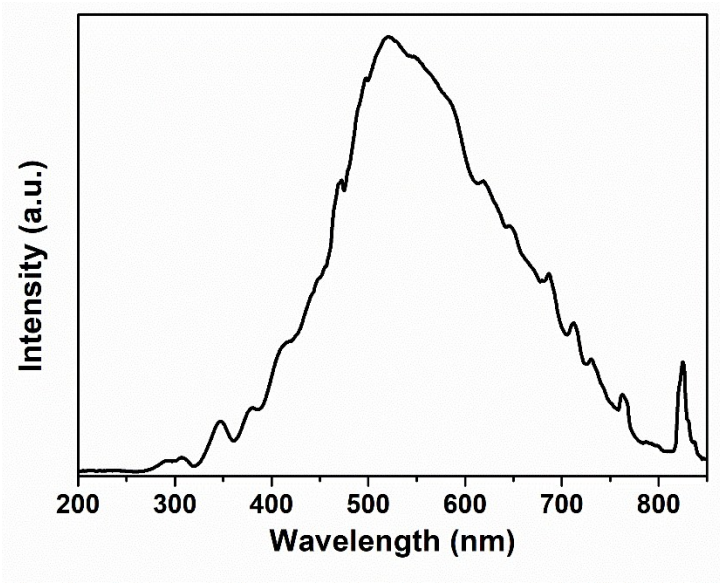

Fig. S1 Spectral distribution of the used light source.

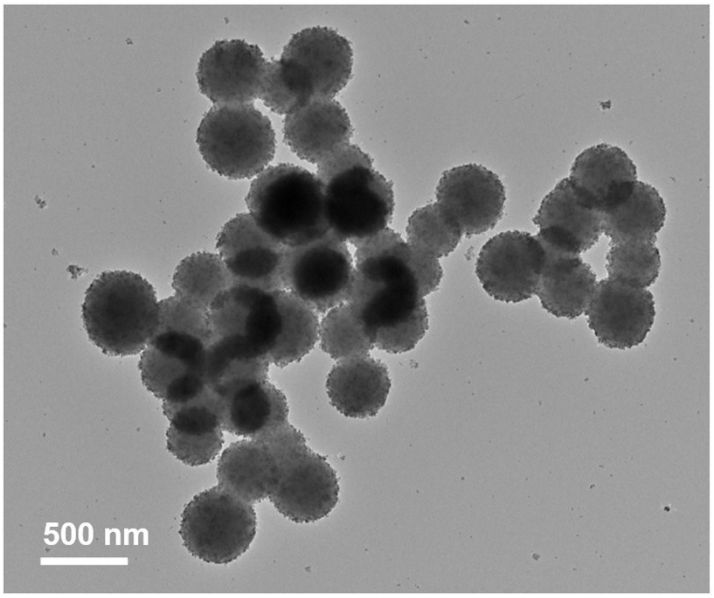

Fig. S2 TEM image of the TiO_2/C sample.

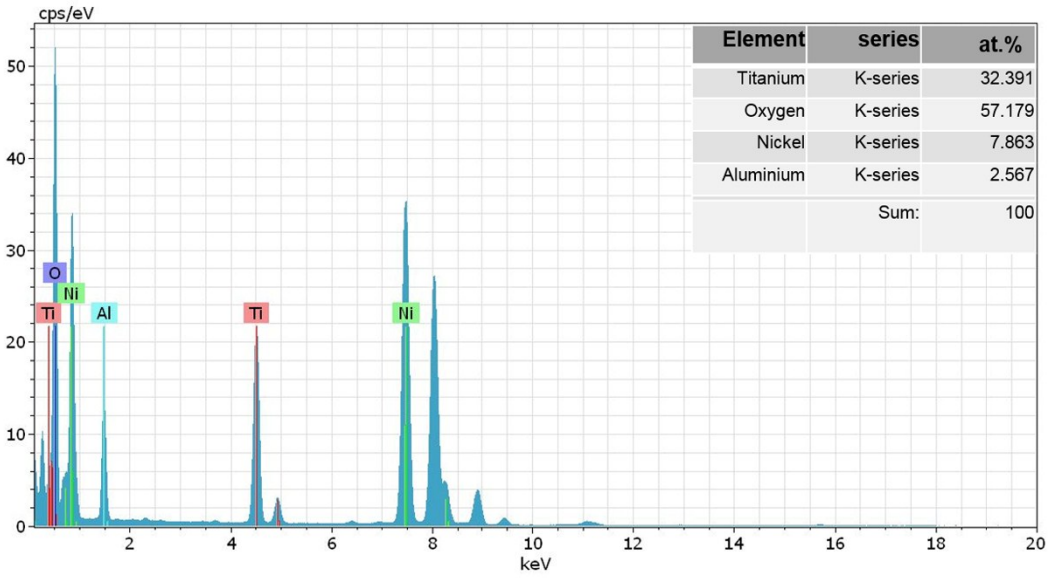

Fig. S3 EDS profile of the TiO_2/LDH core–shell hybrid.

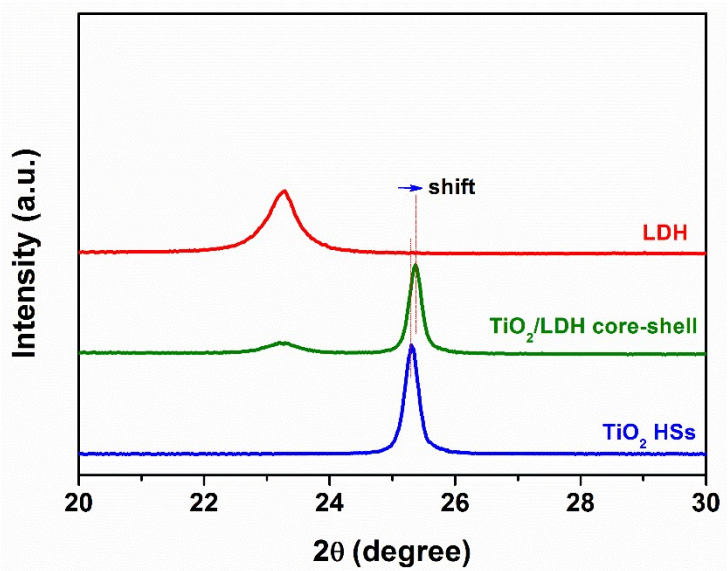

Fig. S4 Magnified XRD spectra of the prepared samples.

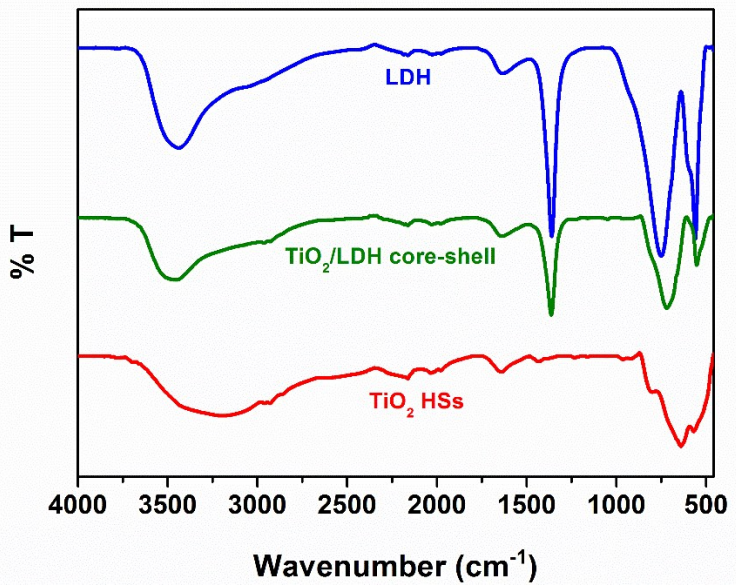

Fig. S5 FT-IR spectra of TiO_2 HSs, LDH, and TiO_2/LDH core–shell hybrid samples.

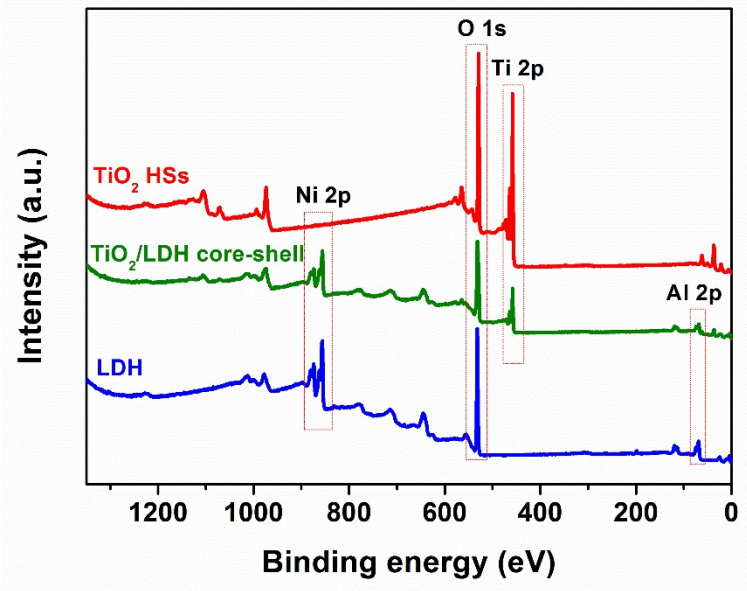

Fig. S6 Survey XPS spectra of TiO_2 HSs, LDH, and TiO_2/LDH core–shell hybrid samples.

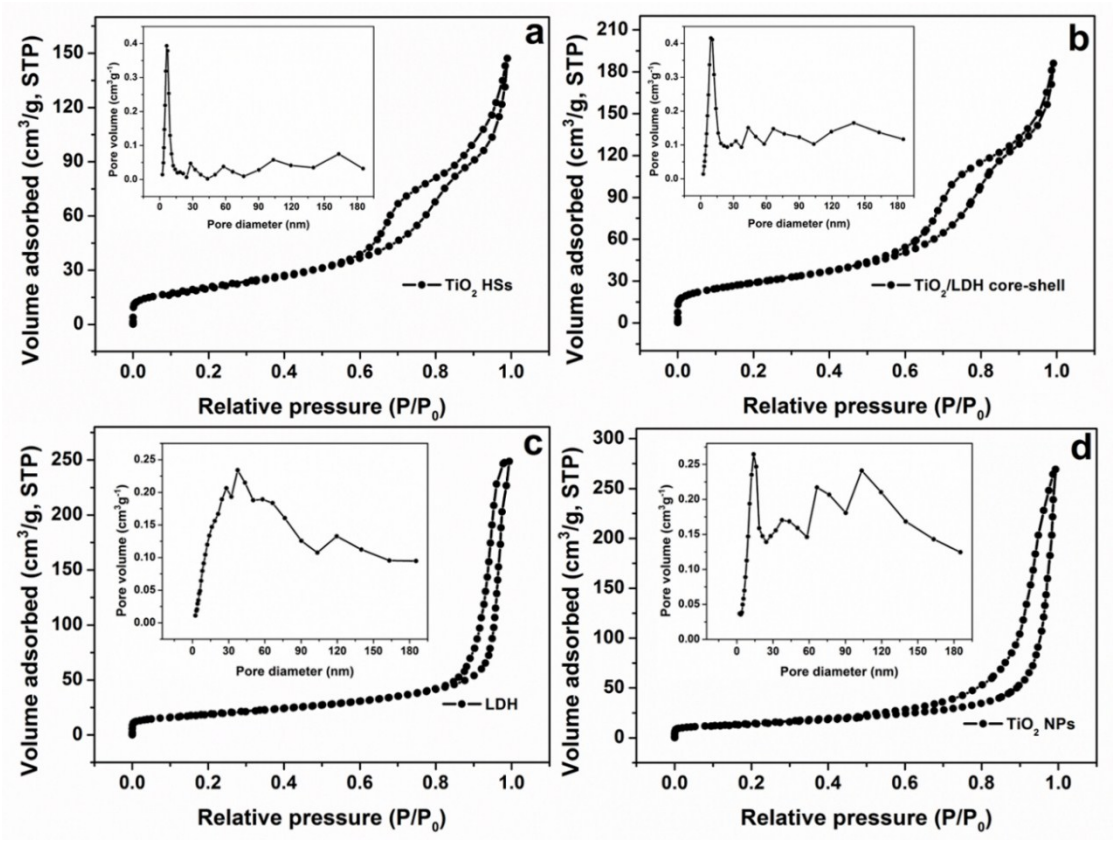

Fig. S7 N_2 adsorption/desorption isotherms and corresponding pore size distribution profiles (the inset) for the (a) TiO_2 HSs, (b) TiO_2/LDH core–shell hybrid, (c) LDH, and (d) TiO_2 NPs samples.

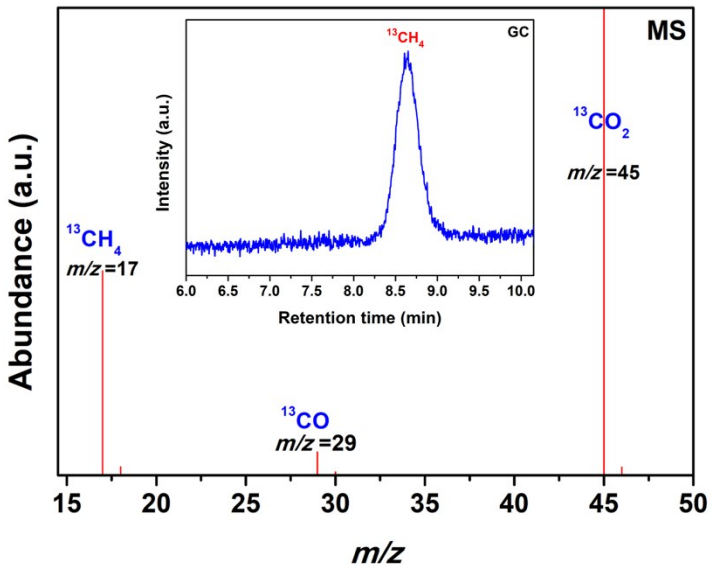

Fig. S8 GC (inset) and MS analyses for the products of photocatalytic $^{13}CO_2$ reduction over the TiO_2/LDH core–shell hybrid after 5 h of light irradiation.

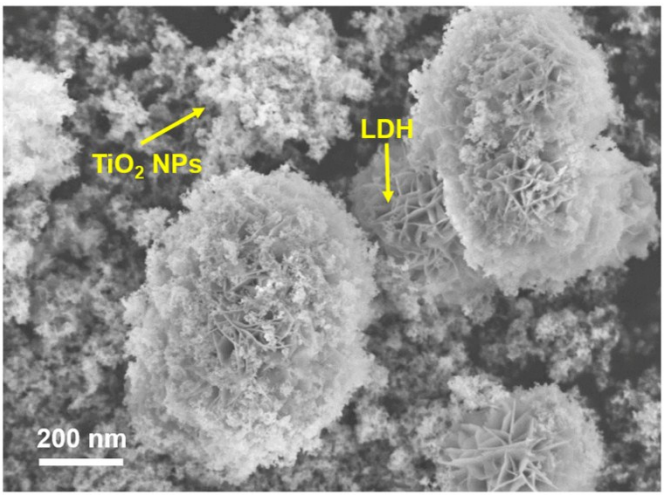

Fig. S9 FESEM image of TiO_2 NPs/LDH sample.

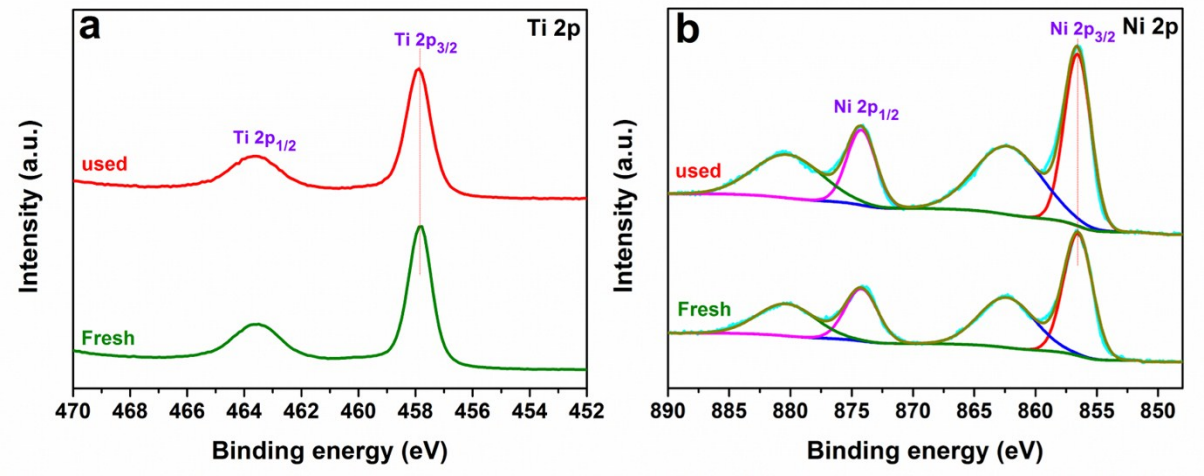

Fig. S10 High-resolution XPS spectra of TiO_2/LDH core–shell hybrid before and after photocatalytic experiments. (a) Ti 2p and (b) Ni 2p.

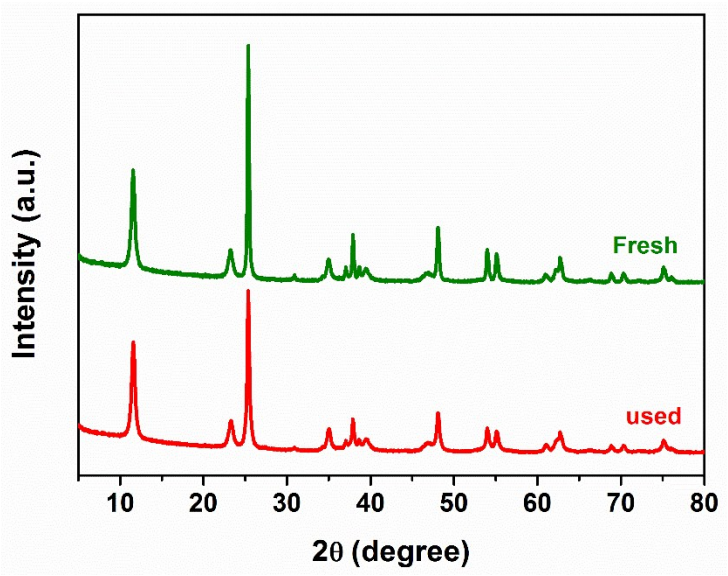

Fig. S11 XRD patterns for TiO_2/LDH core–shell hybrid before and after photocatalytic experiments.

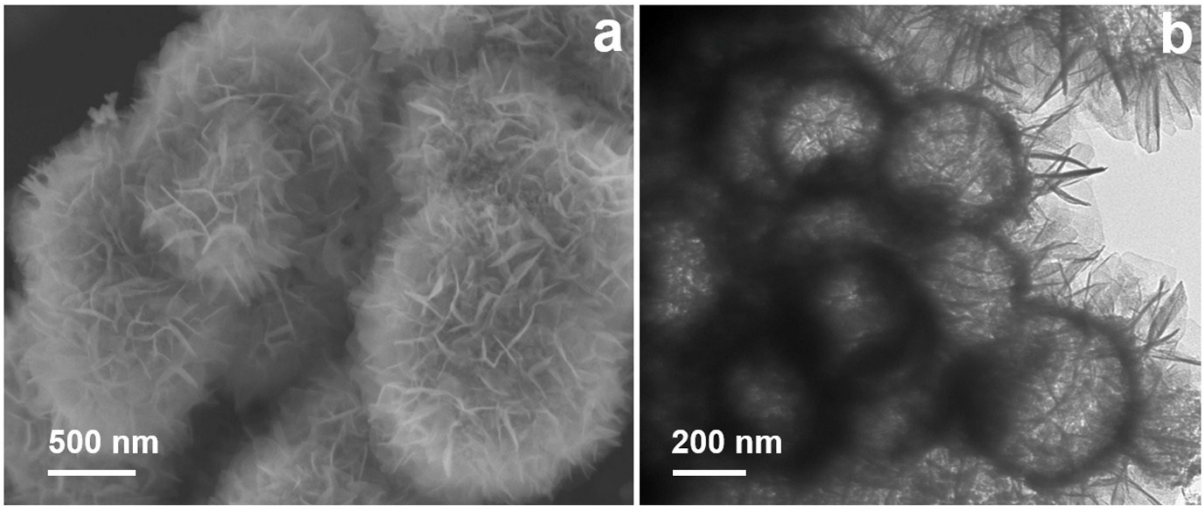

Fig. S12 (a) FESEM and (b) TEM images for TiO_2/LDH core–shell hybrid after photocatalytic experiments.

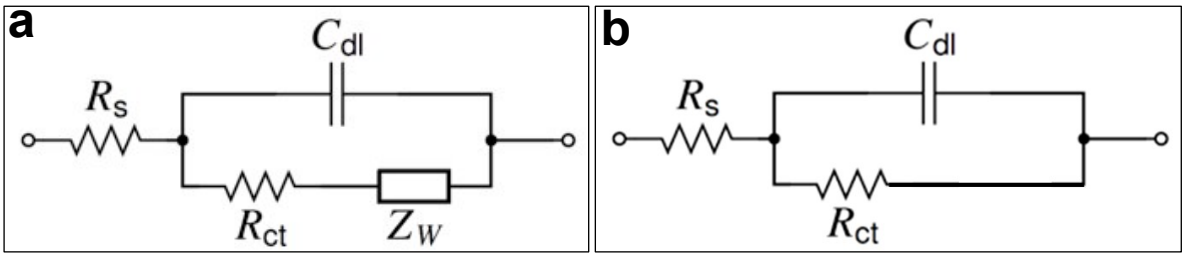

Fig. S13 (a) Randles circuit and (b) simple charge transfer circuit models used for the fitting of the EIS data.

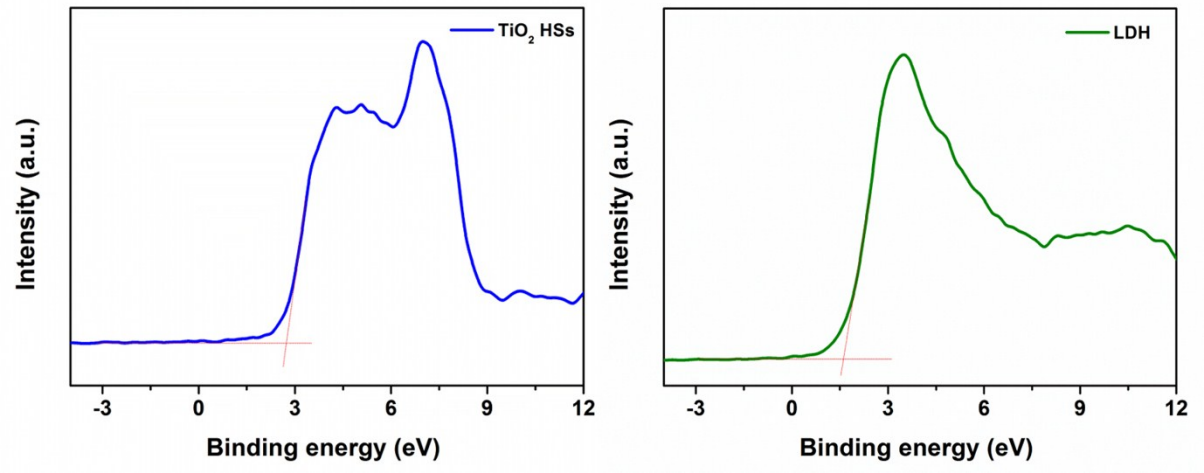

Fig. S14 Valance band XPS profiles of TiO_2 HSs and LDH catalysts.

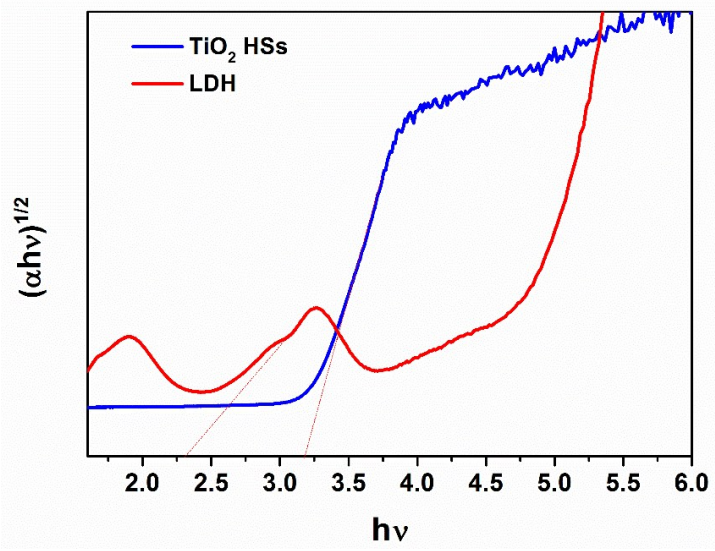

Fig. S15 Tauc plots to determine the optical band gaps of TiO_2 HSs and LDH catalysts.

Table S1 The comparison of photocatalytic CO_2 reduction activities for CH_4 production between TiO_2/LDH core–shell hybrid and other TiO_2-based photocatalysts reported in the literature.

Photocatalyst	**CH_4 production ($\mu mol\ g^{-1}\ h^{-1}$)**	**Reference**
Au/TiO_2	8.0	S1
TiO_2/β Zeolite	5.8	S2
Cu/TiO_2 nanoporous	8.04	S3
Cu_2O–TiO_2-(001)	8.68	S4
Au/TiO_2 yolk–shell	2.52	S5
TiO_2 coexposed (001) and (101)	1.35	S6
Acidified TiO_2 nanosheets	3.3	S7
$Ti_{0.91}O_2$/CdS	10.0	S8
MgO–Pt–TiO_2	11.0	S9
$Zr_xTi_{1-x}O_n$ mixed oxides	0.93	S10
N-TiO_2-(001)/Graphene	0.37	S11
P25/B-doped graphene	1.25	S12
TiO_2/LDH core–shell hybrid	20.56	This work

References

S1 L. Collado, A. Reynal, J.M. Coronado, D.P. Serrano, J.R. Durrant, O. De la Peña, and V.A. Shea, *Appl. Catal. B Environ.*, 2015, **178**, 177–185.

S2 K. Ikeue, H. Yamashita, M. Anpo, and T. Takewaki, *J. Phys. Chem. B*, 2001, **105**, 8350–8355,

S3 T. Zhang, J. Low, and X. Huang, *ChemCatChem*, 2017, **9**, 3054–3062.

S4 S. Zhu, S. Liang, Y. Tong, X. An, J. Long, X. Fu, and X. Wang, *Phys. Chem. Chem. Phys.*, 2015, **17**, 9761–9770.

S5 W. Tu, Z. Yong, H. Li, Z. P. Li, and Z. Zou, *Nanoscale*, 2015, **7**, 14232–14236.

S6 J. Yu, J. Low, W. Xiao, P. Zhou, and M. Jaroniec, *J. Am. Chem. Soc.*, 2014, **136**, 8839–8842.

S7 Z. He, J. Tang, J. Shen, J. Chen, and S. Song, *Appl. Surf. Sci.*, 2016, **364**, 416–427.

S8 W. Tu, Y. Zhou, S. Feng, Q. Xu, P. Li, X. Wang, M. Xiao, and Z. Zou, *Chem. Commun.*, 2015, **51**, 13354–13357.

S9 S. Xie, Y. Wang, Q. Zhang, W. Deng, and Y. Wang, *ACS Catal.*, 2014, **4**, 3644–3653.

S10 K. Kočí, L. Matějová, I. Troppová, and M. Edelmannová, *Catal. Today*, 2017, **287**, 52–58.

S11 W.J. Ong, L.L. Tan, S.P. Chai, S.T. Yong, and A. R. Mohamed, *Nano Res.*, 2014, **7**, 1528–1547.

S12 M. Xing, F. Shen, B. Qiu, and J. Zhang, *Sci. Rep.*, 2014, **4**, 6341.